Eur Phys J C **40**, s02, 33–42 (2005)
Digital Object Identifier (DOI) 10.1140/epjcd/s2005-02-004-2

EPJ C direct
electronic only

Scientific Note

Jet energy correction with charged particle tracks in CMS

O. Kodolova[1,a] (e-mail: Olga.Kodolova@cern.ch), I. Vardanian[2], A. Nikitenko[3,b], L. Fano[4], G. Bruno[1]

[1] CERN, Geneva, Switzerland
[2] Moscow State University, Moscow, Russia
[3] Imperial College, London, UK
[4] Universita degli Studi di Perugia, Italy
[5] CERN, Geneva, Switzerland

Received: 5 September 2004 / Revised: 18 October 2004 /Accepted: 18 October 2004
Published online: 23 March 2005 –

Abstract. The performance of a jet–energy–correction algorithm using reconstructed charged particle tracks is presented. The jet energy correction allows the jet energy scale to be restored and improves the energy resolution for jets with energies up to 120 GeV. For low energy jets (20 GeV) it improves the resolution by a factor 1.7 with respect to uncorrected jets. For 100 GeV jets the resolution improves by 15%. The deviation from unity of the ratio of the reconstructed to the generator jet transverse energies decreases by a factor two for low–E_T jets ($E_T < 30$ GeV). For high–E_T jets, this ratio amounts to 1.00 ± 0.04.

1 Introduction

Physics signatures for SUSY, Higgs bosons, and other processes require reconstruction and measurement of jets coming from high-momentum quarks and gluons, and of the missing transverse energy [1]. The jet energy resolution and linearity is a key factor in separating signal events from background. The main goal is to achieve the best resolution and linearity, i.e. a reconstructed jet energy close to the real jet energy.

The reconstruction of jets is performed in two steps, (i) jet finding with e.g. cone-based algorithms [2]; and (ii) jet energy correction. The factors influencing the reconstructed jet energy can be divided in two groups. One is connected with the jet as a physical object, and includes fragmentation model, initial and final state radiation, the underlying event, and particles coming from additional pile-up events. The second group are factors associated with detector performance. They include electronic noise, magnetic field which deflects low energy charged particles out of the jet reconstruction cone, the responses of the calorimeters to electromagnetic and hadronic showers (e/h ratio), losses due to out-of-cone showering, dead materials and cracks and longitudinal leakage for high energy jets.

Corrections for effects in the first group should be left for the individual channel investigations. Detector effects are more physics–channel independent and common correction coefficients can be provided.

Algorithms for jet energy corrections may be classified according to the different objects that are used for the corrections. The particles generated in a cone of radius R in the (η, ϕ) plane at the production vertex are clustered in a "generator" jet (Fig. 1). "Calorimetric" jets are reconstructed in the calorimeters within a cone of radius R_{reco} in the (η, ϕ) plane. Here, η and ϕ are the pseudorapidity and the azimuthal angle of a jet (generator or reconstructed in the calorimeter).

– **Jet-based corrections**
Corrections are implemented by weighting the energies from the longitudinal calorimeter compartments. One weight can be applied for both the electromagnetic (EC) and hadron (HC) calorimeters:

$$E = \alpha \times (EC + HC)_{in-cone}, \quad (1)$$

or the ECAL and HCAL contributions can have different weights:

$$E = \beta \times EC_{in-cone} + \gamma \times HC_{in-cone}. \quad (2)$$

These weights (α, β, γ) depend on the pseudorapidity (η) and the transverse energy (E_T) of the reconstructed objects and are tuned for different physics objects such as jets of different origin (light quarks, b quarks) or missing E_T. Earlier studies have shown that this method gives an improvement in linearity but the resolution is unchanged [3], and that the two styles of weighting give approximately the same results.

[a] on leave Moscow State University, Moscow, Russia
[b] on leave Institute of Experimental and Theoretical Physics, Russia

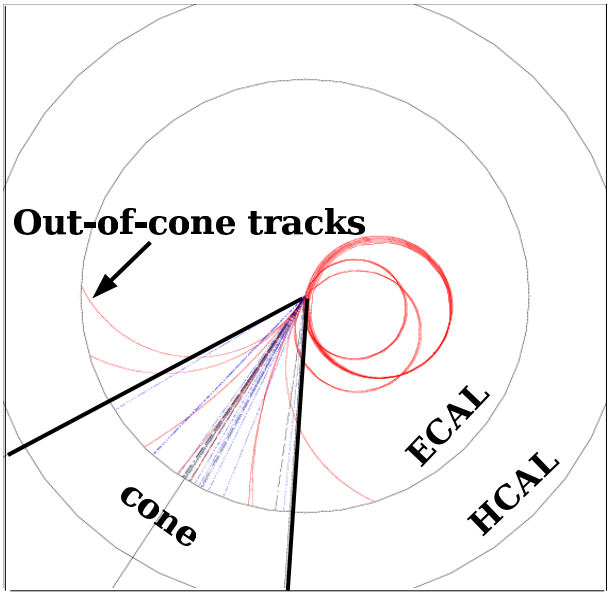

Fig. 1. Single jet in CMS (transverse view). The typical cone size of 0.5 is displayed as black straight lines. The tracks leaving the cone before reaching the calorimeter are called out-of-cone tracks

– **Cluster-based corrections**
Calibration coefficients are applied separately to electromagnetic and hadronic clusters. The clusters found in ECAL and HCAL are separated according to the cluster origin (electron, γ, hadron). Correction coefficients are different for the clusters initiated by electrons and photons, and by hadrons. For electromagnetic clusters, the corrected response is

$$\mathrm{em} = \alpha \times \mathrm{EC}_{\mathrm{cluster}}, \tag{3}$$

and for hadronic clusters, it is

$$\mathrm{had} = \beta \times \mathrm{EC}_{\mathrm{cluster}} + \gamma \times \mathrm{HC}_{\mathrm{cluster}}. \tag{4}$$

The finding and separation of isolated clusters in CMS calorimeters was discussed in [4]. However, the cluster weighting procedure was not investigated.
– **Out-of-cone tracks**
The tracks that are deflected from the jet cone due to magnetic field can be added to the jet energy reconstructed in calorimeter [5]. The correction of energy within the jet cone can be performed with any other procedure.
– **Track based corrections**
The main idea is to replace the energy from identified calorimeter clusters arising from charged particles by the track momenta measured in the inner tracking detector. A considerable improvement of the calorimeter jet energy resolution with the use of the reconstructed tracks (energy flow algorithm) has been already demonstrated in a number of HEP experiments at LEP [6], Tevatron [7] and HERA [8]. The use of the tracker information as developed for CMS [4,9] is described in this note and is found to be promising.

The "jet-based" method is very useful in the Level-1 trigger, where there is no possibility to use tracker information. In the High-Level trigger, however, some information from the measured tracks is available. Full use of the tracker information for energy corrections is possible only in off-line analysis.

2 The CMS detector

A characteristic feature of the CMS detector is its large superconducting solenoid delivering an axial magnetic field of 4 T. The hadron and electromagnetic calorimeters are located inside the coil (except the forward calorimeter) and cover the pseudorapidity range $|\eta| < 5$ [10,11]. The calorimeters are designed to allow jet reconstruction in the full pseudorapidity region. The calorimeter extends to $\eta = 5$, but jets can be measured if their axes lie in the range $|\eta| < 4.5$. At $\eta = 5$, half the jet will be lost. In addition, the CMS detector has a silicon tracker ($|\eta| < 2.4$) which allows track momenta to be determined with a resolution better than 1% for low–p_T tracks (p_T between 0.5 GeV and a few tens of GeV) [12].

2.1 Calorimeter segmentation

In the barrel and most of the endcap part of HCAL, the size of the towers is $\Delta\eta = 0.0870$ by $\Delta\phi = 2\pi/72 \approx 0.0873$ rad. At high η in the HCAL endcap ($|\eta| > 1.74$), the towers become larger in η and double the size in ϕ. The granularity of the crystals in the ECAL barrel is $\Delta\eta \times \Delta\phi = 0.0175 \times 0.0175$ rad, which corresponds to a crystal front face of about 20×20 mm^2. In the ECAL endcap ($1.48 < |\eta| < 3.0$), the (η, ϕ) granularity increases progressively to a maximum value of $\Delta\eta \times \Delta\phi = 0.05 \times 0.05$ rad, while the crystal size of 28×28 mm^2 remains the same. There is no longitudinal segmentation in the ECAL and in the barrel part of the HCAL except at the barrel–endcap transition region. The HCAL endcap has two or three segments in depth.

2.2 Tracking detectors

The tracker is composed of two different types of detectors, pixels and silicon strips. The pixel detector consists of three barrel layers located at 4, 7 and 11 cm from the beam axis with granularity 150×150 μm^2 and two forward layers with granularity 150×300 μm^2 located at 34 and 43 cm in z from the centre of the detector.

The silicon strip detectors are divided into inner and outer sections and fill the tracker area from 20 to 110 cm (ten layers) in the transverse direction and up to 260 cm (twelve layers) in longitudinal direction. The strip lengths for the silicon strip sensors vary up to 21 cm for the outermost layers and the pitch varies from 61 to 205 μm depending on the radius. The η-coverage of the tracker is $|\eta| < 2.4$.

2.3 Detector simulation

The CMS detector was described in detail using CMSIM1.25 [13] based on GEANT3. The event reconstruction was performed with ORCA6.31 [14]. For the reconstruction of the energy deposition in the hadron calorimeter, calibration constants obtained with the hadron shower model GHEISHA (in GEANT3) were used. They were determined with the initial transverse energy of pion (E_T) of 50 GeV and pseudorapidity range $0.05 < \eta < 0.3$ for the barrel and $1.8 < \eta < 2.2$ for the endcap part of the calorimeters. The energy cuts (GEANT cuts), below which the particle is stopped, were 1 MeV for electrons and photons and 1 MeV for hadrons. For the tracking detectors, the GEANT cuts were lowered to 100 keV for electrons and 1 MeV for hadrons.

3 Jet energy corrections using the tracker

The CMS ECAL and HCAL have a different response for electron/photons and hadrons. The energy/momentum ratio of the HCAL was measured to be 85 % for 30 GeV pions in the test beam. The ratio of the reconstructed energy to the beam energy is presented in Fig. 2, assuming that for electromagnetic showers this ratio is unity in the full dynamic range [15,16]. The charged particle tracks with transverse momentum less then 1 GeV/c are swept away from the jet reconstruction cone (out-of-cone tracks) because of the 4 T magnetic field. The strong field shifts other charged particles from the jet core, resulting in a better separation of the charged energy clusters and neutral energy clusters (Fig. 1). In this study the jet cone radius R at the production vertex coincides with the jet reconstruction cone radius R_{reco} in the calorimeters.

Using the tracker information, several corrections can be applied to improve the calorimeter response. These corrections may be applied individually or in combination.

A response subtraction procedure was proposed in [9]. For each track reaching the calorimeter surface within the reconstruction cone, (Fig. 1), the expected response is subtracted from the calorimeter jet energy and the track momentum is used instead. The expected response to charged particles in the calorimeters can be estimated and tabulated either with a sample of isolated tracks simulated at different energies or with test beam data (Sect. 3.1.2). This subtraction procedure does not require cluster separation and is therefore well suited to the case of high occupancy or coarse granularity. The momenta of the tracks that reach the calorimeter surface out of the reconstruction cone are simply added to the calorimeter jet energy.

In addition to the response subtraction procedure, the charged particle momenta could also be used to replace the energies of the calorimeter clusters compatible with the track extrapolation [4,9]. This possibility is not included in the current algorithm design and is not considered in the present study.

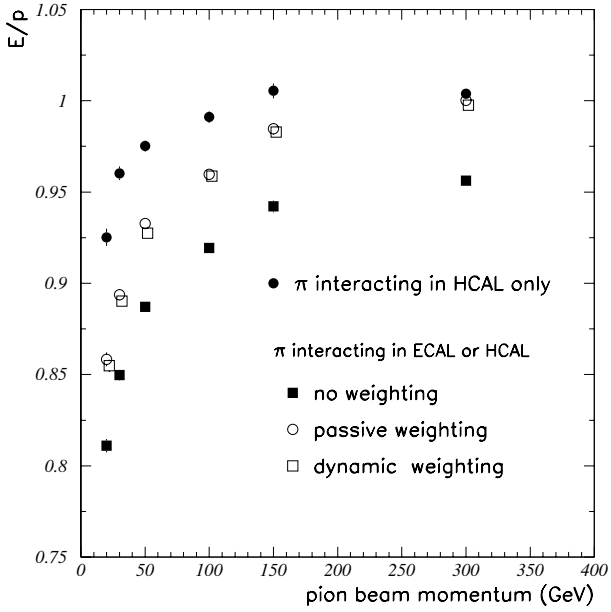

Fig. 2. Ratio of the energy (E) measured in ECAL and HCAL to the initial pion energy (p) from test beam data [16]. Pions interacting only in HCAL (close circle); pions interacting in ECAL or HCAL; without applying the coefficient to the calorimeter readouts, i.e. without readout weighting (close squares); with passive weighting, i.e., constant coefficient independent on energy only to the first HCAL readout, the coefficients to the other readouts assumed to be equal to one (empty circles); dynamic weighting, i.e. event–by–event correction coefficient to ECAL readout depending on the fraction of energy deposited in the first HCAL readout relative to the total deposited energy in HCAL (empty squares)

3.1 Algorithm description

3.1.1 Response subtraction procedure and out-of-cone tracks

The following corrections are made for each jet found in the calorimeter.

- The event vertex is found with the use of pixel track segments [2]. The pixel track segments originating from the event vertex and within the jet reconstruction cone are used as seeds for the Combinatorial Track Finder [17]. Tracks are required to have $p_T > 1$ GeV/c.
- Out-of-cone tracks satisfy the following criteria
  - $\Delta R_v < R_{reco}$,
  - $\Delta R_c > R_{reco}$,

  where ΔR_v is the distance in the (η, ϕ) plane between the calorimeter jet axis and the track direction at the production vertex, and ΔR_c is the distance between the jet axis and the expected impact point of the track on the calorimeter surface. The momenta of these tracks, reconstructed in the tracker, $E_{tracks}^{out-of-cone}$, are added to the jet energy, E_{jet}^{reco}, reconstructed in the calorimeter.

$$E_{jet}^{corrected} = E_{jet}^{reco} + E_{tracks}^{out-of-cone}. \quad (5)$$

– The momentum of each reconstructed track with an ECAL impact point inside the cone (Fig. 1) is measured in the tracker. The expected response in the calorimeters is obtained from a parametrization and then subtracted from the jet energy [9]. The track momentum is instead added to the jet energy. Before the subtraction, the reconstructed jet energy is

$$\mathrm{E}_{\mathrm{jet}}^{\mathrm{reco}} = \mathrm{EC}_{e/\gamma} + (\mathrm{EC}+\mathrm{HC})_{\text{neutral hadrons}} + (\mathrm{EC}+\mathrm{HC})_{\text{charged hadrons}}, \quad (6)$$

where $(\mathrm{EC}+\mathrm{HC})_{\text{neutral hadrons}}$ and $(\mathrm{EC}+\mathrm{HC})_{\text{charged hadrons}}$ are the responses of the electromagnetic and the hadron calorimeters to neutral and charged hadrons, and $\mathrm{EC}_{e/\gamma}$ is the response of the electromagnetic calorimeter to electrons and photons, respectively.
Assuming that all tracks are recontructed, the reconstructed jet energy becomes, after subtraction

$$\mathrm{E}_{\mathrm{jet}}^{\mathrm{corrected}} = \mathrm{EC}_{e/\gamma} + (\mathrm{EC}+\mathrm{HC})_{\text{neutral hadrons}} + \mathrm{E}_{\mathrm{tracks}}^{\mathrm{in-cone}}. \quad (7)$$

After the addition of out-of-cone tracks, the final expression is

$$\mathrm{E}_{\mathrm{jet}}^{\mathrm{corrected}} = \mathrm{EC}_{e/\gamma} + (\mathrm{EC}+\mathrm{HC})_{\text{neutral hadrons}} + \mathrm{E}_{\mathrm{tracks}}^{\mathrm{in-cone}} + \mathrm{E}_{\mathrm{tracks}}^{\mathrm{out-of-cone}}. \quad (8)$$

The track reconstruction inefficiency leads to the appearence of an additional term in the expression for the corrected jet energy

$$\mathrm{E}_{\mathrm{jet}}^{\mathrm{corrected}} = \mathrm{EC}_{e/\gamma} + (\mathrm{EC}+\mathrm{HC})_{\text{neutral hadrons}} + \mathrm{E}_{\mathrm{tracks}}^{\mathrm{in-cone}} + \mathrm{E}_{\mathrm{tracks}}^{\mathrm{out-of-cone}} + (\mathrm{EC}+\mathrm{HC})_{\text{charged hadrons}}^{\text{no track}}. \quad (9)$$

The variance of the distribution of $\mathrm{E}_{\mathrm{jet}}^{\mathrm{corrected}}$ can be expressed with the formula:

$$\mathrm{D}(\mathrm{E}_{\mathrm{jet}}^{\mathrm{corrected}}) = \mathrm{D}(\mathrm{E}_{\mathrm{jet}}^{\mathrm{reco}}) + \sum_{\text{tracks out of cone}} \mathrm{D}(\mathrm{E}_{\mathrm{track}}^{\text{out of cone}}) + \sum_{\text{tracks in cone}} \mathrm{D}(\mathrm{E}_{\mathrm{track}}^{\mathrm{expected}}) + \sum_{\text{tracks in cone}} D(E_{\mathrm{track}}^{\text{in cone}}) \quad (10)$$

$\mathrm{D}(\mathrm{E}_{\mathrm{tracks}}^{\text{in cone}})$ and $\mathrm{D}(\mathrm{E}_{\mathrm{tracks}}^{\text{out of cone}})$ are defined by the tracker resolution which is negligible ($< 0.01 * \mathrm{P}_{\mathrm{T}}^{\mathrm{track}}$) in comparison with $\mathrm{D}(\langle \mathrm{E}_{\mathrm{jet}}^{\mathrm{reco}} \rangle)$. $\mathrm{D}(\langle \mathrm{E}_{\mathrm{tracks}}^{\mathrm{expected}} \rangle)$ will go to zero as the size of the sample of prompt isolated particles is increased.

The jet energy resolution is defined with the formula

$$\mathrm{Resolution}(\mathrm{E}) = \sigma\left(\frac{\mathrm{E}_{\mathrm{jet}}^{\mathrm{reco}}}{\mathrm{E}_{\mathrm{jet}}^{\mathrm{gene}}}\right) \Big/ \left\langle \frac{\mathrm{E}_{\mathrm{jet}}^{\mathrm{reco}}}{\mathrm{E}_{\mathrm{jet}}^{\mathrm{gene}}} \right\rangle, \quad (11)$$

where $\mathrm{E}_{\mathrm{jet}}^{\mathrm{gene}}$ is the energy of generator jet.

The transverse jet energy resolution is defined with the formula

$$\mathrm{Resolution}(\mathrm{E_T}) = \sigma\left(\frac{\mathrm{E}_{\mathrm{Tjet}}^{\mathrm{reco}}}{\mathrm{E}_{\mathrm{Tjet}}^{\mathrm{gene}}}\right) \Big/ \left\langle \frac{\mathrm{E}_{\mathrm{Tjet}}^{\mathrm{reco}}}{\mathrm{E}_{\mathrm{Tjet}}^{\mathrm{gene}}} \right\rangle \quad (12)$$

Taking into account that the polar angle of jet direction θ is limited to the range from 15 degrees to 90 degrees and assuming that $\langle \mathrm{E}\ \sin(\theta) > \ \simeq \langle \mathrm{E} \rangle \langle \sin(\theta) \rangle$, the transverse jet energy resolution can be expressed with the formula

$$\mathrm{Resolution}(\mathrm{E_T}) \ \simeq \sqrt{\mathrm{Resolution}^2(\mathrm{E}) + \cot^2(\theta) \times \mathrm{D}(\theta)}, \quad (13)$$

where θ is the polar angle of jet direction and Resolution(E) is defined with the formula 11.

The procedure increases the jet energy due to an exchange of the underestimated response of calorimeters to charged hadrons with the momentum of the track in the tracker and adding the out-of-cone energy. The variance is kept at the same value. The procedure results in decreasing the first term of formula 13. The direction of jet is also corrected with use of the primary vertex position and charged particles trajectory parameters. The correction of jet direction leads to decreasing the second term of formula 13. The relative weights of the first and second terms in formula 13 depends on the polar angle θ. The first term plays the main role in the barrel part of the CMS detector while the second term dominates in the endcap.

The systematic shift $\delta\mathrm{E}^{\mathrm{syst}} = \langle \mathrm{E}_{\mathrm{jet}}^{\mathrm{corrected}} \rangle - \langle \mathrm{E}_{\mathrm{jet}}^{\mathrm{gene}} \rangle$ has two possible origins, denoted $\delta\mathrm{E}_1$, $\delta\mathrm{E}_2$. The $\delta\mathrm{E}_1$ contribution results from the uncertainty in the expected response parametrization. The $\delta\mathrm{E}_2$ shift arises from neutral hadrons (and, equivalently, from charged hadrons with no associated track), the response of which is not corrected a posteriori.

3.1.2 Determination of the calorimeter expected response to charged particles

Two different methods were tested to determine the calorimeter expected response to charged particles. Both are based on measurements made with single isolated particles.

– e/π technique
The expected response can be calculated from the e/π ratio measured for different energies with sets of isolated particles [15,18]. Isolated particles can be identified during the data taking. The ratio of the amounts of energies deposited in ECAL and HCAL has to be evaluated. The response in ECAL is different if the particles interact in the ECAL hadronically or not. The interacting and non-interacting particles are disentangled by measuring the energy deposited in a 3×3 array of crystals ($E_{3\times3}$) around the impact point. If $\mathrm{E}_{3\times3}$ <0.5 GeV, the particle is called a non-interacting particle, and the measured $\mathrm{E}_{3\times3}$ energy is taken as the "expected" response in the ECAL. The expressions for

Table 1. Expected response for charged particles

	The particle interacts in ECAL	The particle does not interact in ECAL
$EC_{\text{charged hadrons}}$	p_{track}*f(p_{track})/$(e/\pi)_{ECAL}$	$E_{3\times3}$
$HC_{\text{charged hadrons}}$	p_{track}*(1-f(p_{track}))/$(e/\pi)_{HCAL}$	$(p_{track} - E_{3\times3})/(e/\pi)_{HCAL}$

the expected response to charged particles are given in Table 1 as functions of the particle momentum p_{track}. The e/π ratio in ECAL and HCAL is calculated with the following expressions [18]

$$(e/\pi)_{ECAL} = (e/h)_{ECAL}/\{1 + [(e/h)_{ECAL} - 1] \times F_{ECAL}\}, \quad (14)$$

$$(e/\pi)_{HCAL} = (e/h)_{HCAL}/\{1 + [(e/h)_{HCAL} - 1] \times F_{HCAL}\}, \quad (15)$$

where $(e/h)_{ECAL} = 1.6$, $(e/h)_{HCAL} = 1.39$ are obtained from test beam data analysises (300 GeV pion beam [16]). The quantities F_{ECAL}, F_{HCAL} are the expected ECAL and HCAL deposited energy fraction for the hadronic showers and are evaluated as: $F_{ECAL(HCAL)} = 0.11 \times \log(E_{ECAL(HCAL)})$ [18]. The ratio $f(p_{track}) = E_{ECAL}/p_{track} = 0.4$ was used to account for the fraction of charged particle energy deposited in the ECAL as determined from the same test beam data [15].

– Library of responses

The p_T dependence of the mean responses in the ECAL and HCAL isolated pions interacting in ECAL is shown in Figs. 3 and 4. The p_T dependence for particles not interacting in ECAL is shown in Fig. 5 .

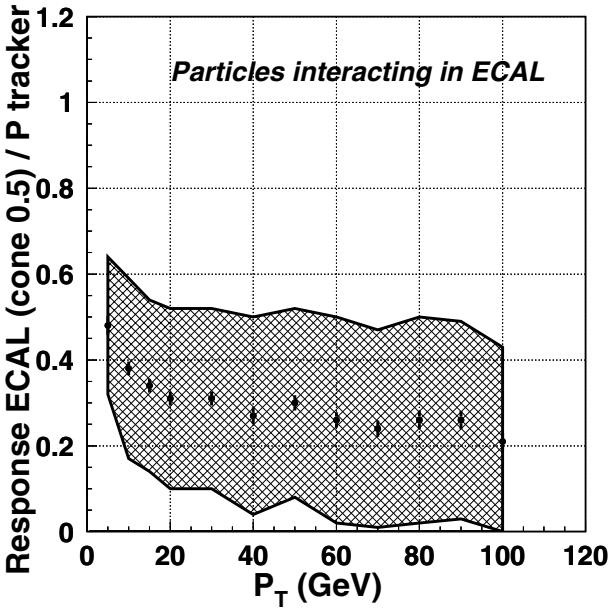

Fig. 3. Ratio of the mean response in ECAL to the original particle energy for isolated pions interacting in the ECAL as a function of the particle transverse energy for $|\eta| < 0.3$. The hatched area corresponds to the RMS of the ratio distribution at that energy

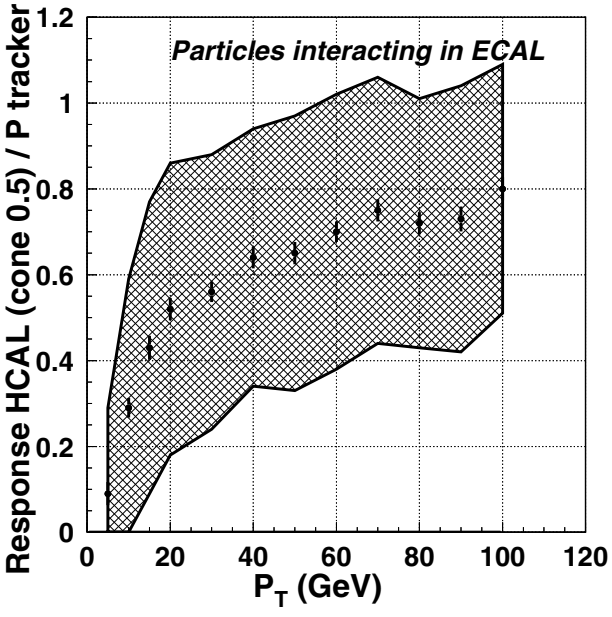

Fig. 4. Ratio of the mean response in HCAL to the original particle energy for isolated pions interacting in the ECAL as a function of the particle transverse energy for $|\eta| < 0.3$. The hatched area corresponds to the RMS of the ratio distribution at that energy

3.2 Algorithm performance

The algorithm performance is evaluated with the library of responses constructed with generated single particle samples. The e/π technique requires test beam data with different beam energies to estimate $f(E_{track})$.

3.2.1 Reconstruction of single jet

Samples of QCD di-jet events in different intervals of the initial parton transverse momentum, $\hat{p}_T$, were simulated with Pythia 6.158 [19]. At the generator level, jets are found with a simple cone algorithm ($R = 0.5$) around the leading particle in the jet. Particles belonging to the jet are passed through the complete detector simulation; other particles in the event are ignored. The calorimeter digitization is done in the no pile-up scenario.

Calorimeter jets and jets at particle level (generator jets) are reconstructed within a cone of radius $R = 0.5$ with the iterative cone algorithm [2]. The generator jets do not include muons and neutrinos. Reconstructed jets are compared with generator jets. The comparison is focused on the detector effects and is somewhat insensitive

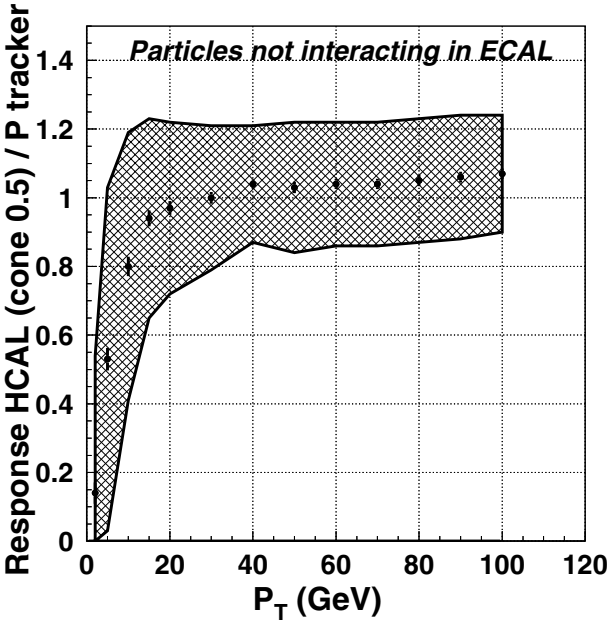

Fig. 5. Ratio of the mean response in HCAL to the original particle energy for isolated pions not-interacting in the ECAL as a function of the particle transverse energy for $|\eta| < 0.3$. The hatched area corresponds to the RMS of the ratio distribution at that energy

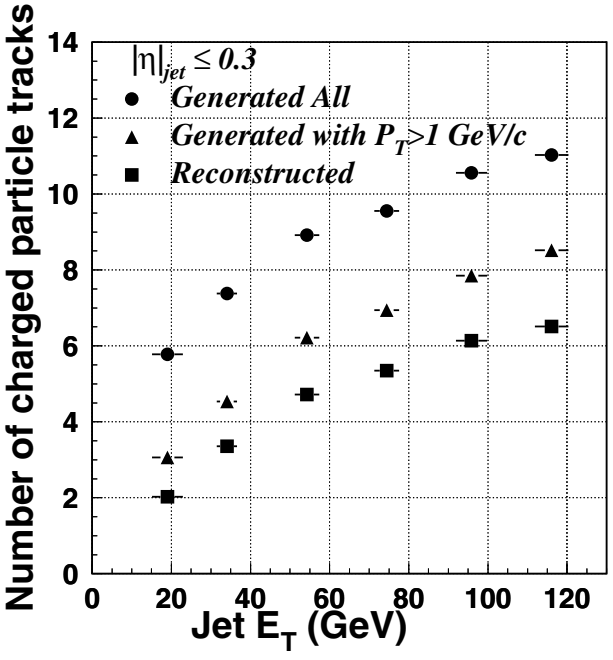

Fig. 6. The mean number of generated and reconstructed charged particles in barrel jets ($|\eta| < 0.3$) as a function of jet energy. Circles – the generated charged particles with no p_T cut applied. Triangles – the generated charged particles with $p_T > 1$ GeV/c. Squares – the reconstructed tracks.

to effects of initial and final state radiation as well as of underlying and pile-up events.

The quality of the track reconstruction plays an important rôle. The mean number of generated and reconstructed tracks in a cone R_{reco} as a function of the generator jet energy is presented in Figs. 6 and 7. No p_T cut was applied on the momentum of generated particles. The cut on p_T for reconstructed tracks is 1 GeV/c. Four tracks per jet are lost on average irrespective of the jet energy. Low-E_T jets are most affected because the fraction of low energy particles is higher in low–energy jets than in high–energy jets.

The energy resolution (13) and the reconstructed energy dependence on the generated transverse energy are shown in Figs. 8 and 9 for jets generated with $|\eta| < 0.3$. When the jet energy corrections are applied, the reconstructed jet energy fraction for 20 GeV generator jets increases from 0.5 to 0.85 and the same fraction for 120 GeV jets increases from 0.87 to 1.03. For jet energies from 50 to 120 GeV, the non-linearity is within 8%. The variation of the resolution and linearity arising from the inclusion of out-of-cone tracks is presented in the same figures. The resolution improves by about 30% as a result of adding the out-of-cone tracks.

In the endcap region (Figs. 10 and 11), jets with the same E_T as in the barrel are more energetic. The energy of jets with E_T=30 GeV in the endcap corresponds to that of jets with E_T=90 GeV in barrel. In addition, the tracking efficiency is smaller in the endcap than in the barrel. Therefore, the tracker information is not relevant in the endcap above 80–90 GeV and is less rewarding for lower E_T jets than in the barrel.

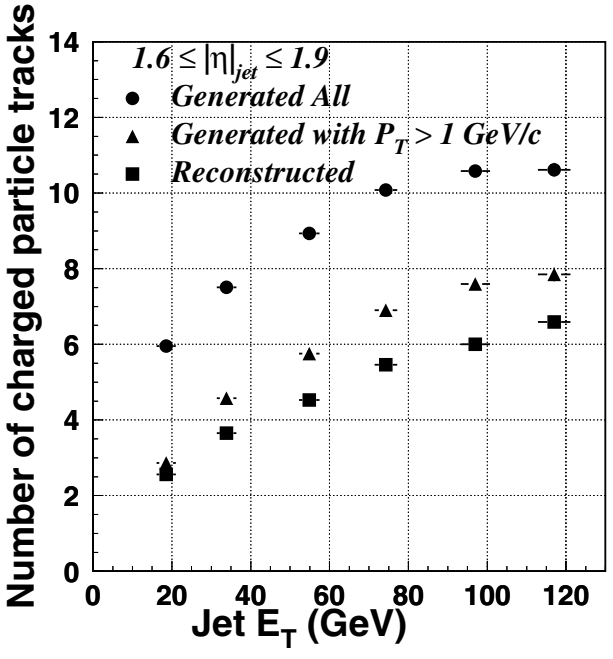

Fig. 7. The mean number of generated and reconstructed charged particles in barrel jets ($1.6 < |\eta| < 1.9$) as a function of jet energy. Circles – the generated charged particles with no p_T cut applied. Triangles – the generated charged particles with $p_T > 1$ GeV/c. Squares – the reconstructed tracks

3.2.2 Reconstruction of dijet events

Di-jet events with $\hat{p}_T$ between 80 and 120 GeV/c were generated with PYTHIA 6.158, fully simulated with CMSIM,

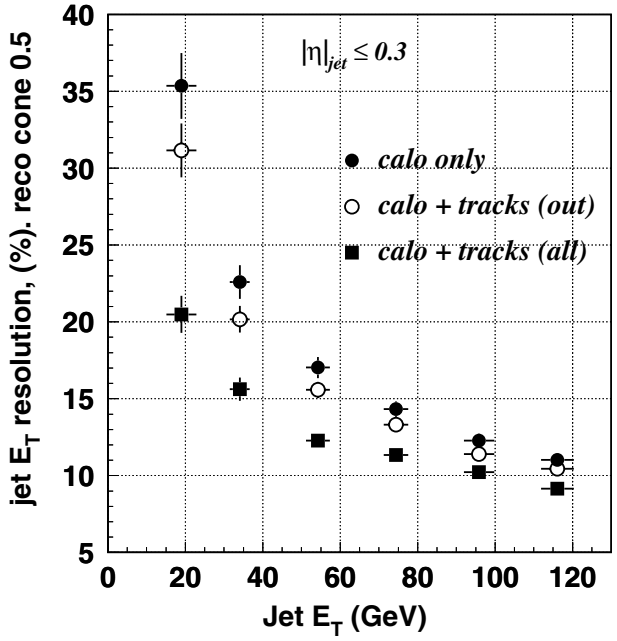

Fig. 8. The jet transverse energy resolution as a function of the original jet transverse energy in a single jet sample; reconstruction with calorimeter only (close circles), out-of-cone tracks (open circles), subtraction procedure of expected responses using library of responses (close squares)

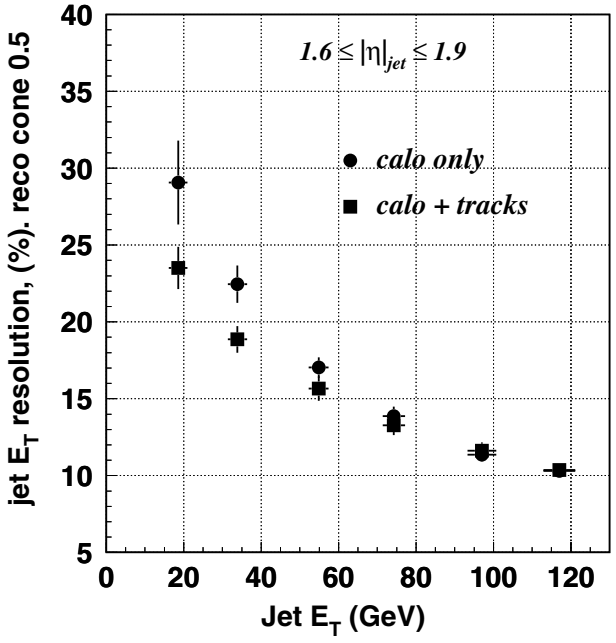

Fig. 10. The jet transverse energy resolution as a function of the original jet transverse energy in a single jet sample; reconstruction with calorimeter only (close circles), subtraction procedure of expected responses using library of responses and out-of-cone tracks (close squares)

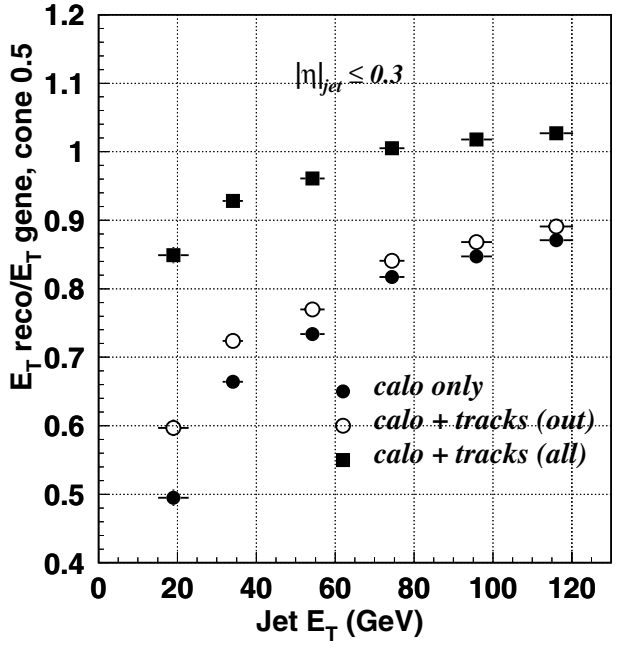

Fig. 9. The reconstructed jet transverse energy as a function of the generator jet transverse energy. The symbols are the same as in Fig. 8

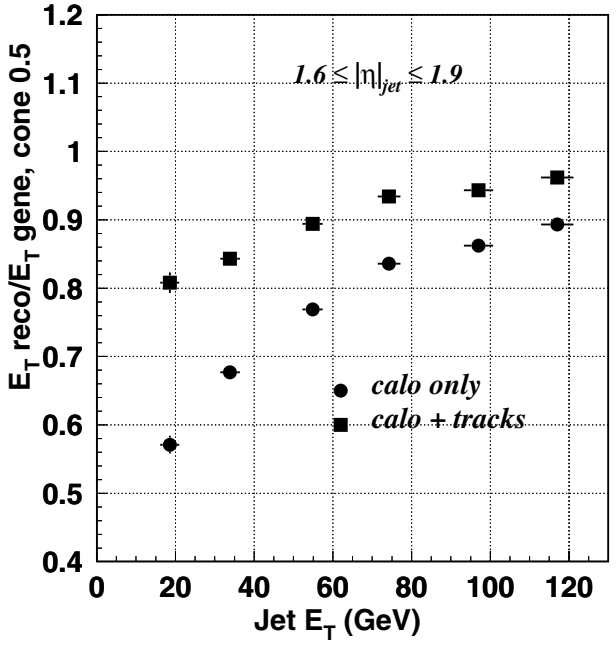

Fig. 11. The reconstructed jet transverse energy as a function of the generator jet transverse energy. The symbols are the same as in Fig. 10

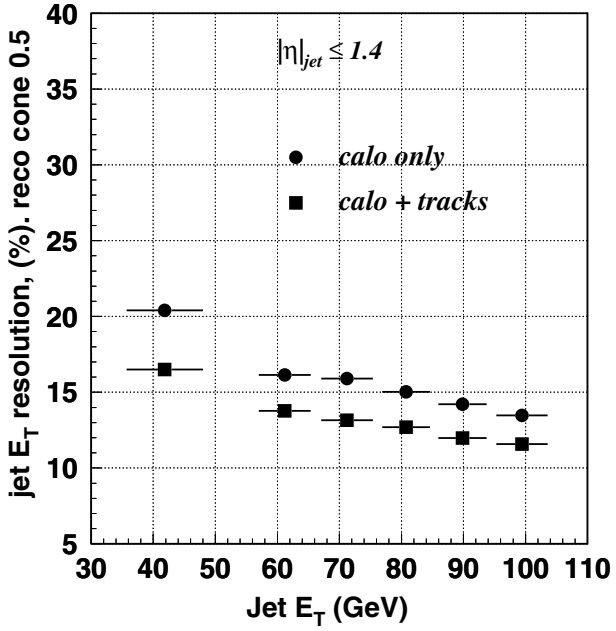

Fig. 12. Jet transverse energy resolution as a function of the generator jet transverse energy for jets with $0 < |\eta| < 1.4$ (barrel) from a sample with low luminosity pile-up; reconstruction with calorimeter only (close circles), subtraction procedure of expected responses using library of responses and out-of-cone tracks (close squares)

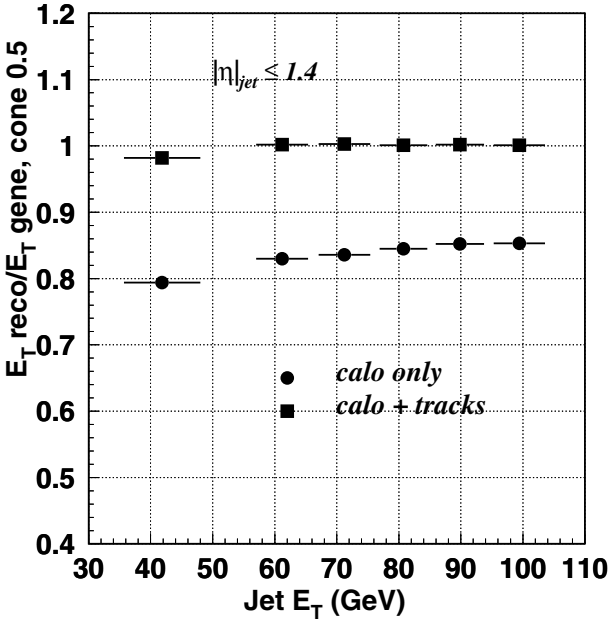

Fig. 13. Reconstructed jet transverse energy as a function of the generator jet transverse energy. The symbols are the same as in Fig. 12

digitized and reconstructed in low luminosity conditions ($L = 2 \times 10^{33} cm^{-2} s^{-1}$). The resolution and the reconstructed jet energy fraction are shown for jets generated with $|\eta| < 1.4$ in Figs. 12 and 13 and in the endcaps in Figs. 14 and 15. This sample was simulated with pile-up events and no special procedures to suppress pile-up energy was used. The resolution improvement is the same as for single jets with no pile-up. A larger amount of energy is however present in the jet cone R_{reco}. This amount is the same for all jet energies and corresponds to the energy flow average from the pile-up events. The additional energy affects lower–energy jets more than higher–energy jets. The dependence on the generator transverse jet energy is therefore less pronounced. Jets in the endcap are more affected by pile-up than in the barrel.

3.2.3 Reconstruction of the X → jj (120 GeV/c^2) mass

Events with a 120 GeV/c^2 X object decaying into light quarks with initial state and final state radiation were fully simulated, digitized and reconstructed for low luminosity pile-up conditions. The X mass is reconstructed from the two leading jets that are within R = 0.5 of the direction of the primary partons. The generated dijet mass is presented in Fig. 16. The mass peak is at 115 GeV/c^2 and the mean value is 110 GeV/c^2. The same jets reconstructed in the calorimeters only give the mass peak at 96 GeV/c^2 (Fig. 17). A ratio of the X mass reconstructed to the X mass generated for calorimetry jets and calorimeter-plus-tracker jets is shown in Fig. 18.

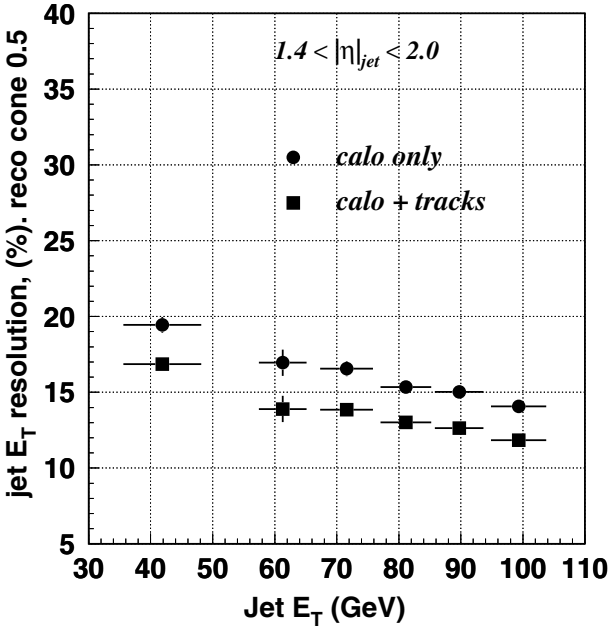

Fig. 14. Jet transverse energy resolution as a function of the generator jet transverse energy for jets with $1.4 < |\eta| < 2$ (endcap) from a sample with low luminosity pile-up; reconstruction with calorimeter only (close circles), subtraction procedure of expected responses using library of responses and out-of-cone tracks (close squares)

The di-jet mass is restored with a systematic shift of about 1% and the resolution is improved by 10%. The ratio of the reconstructed to the generated X mass is 0.88 before corrections with tracks and 1.01 after corrections. The calculation of the pile-up events contribution to the mass spectrum is done with a simple esti-

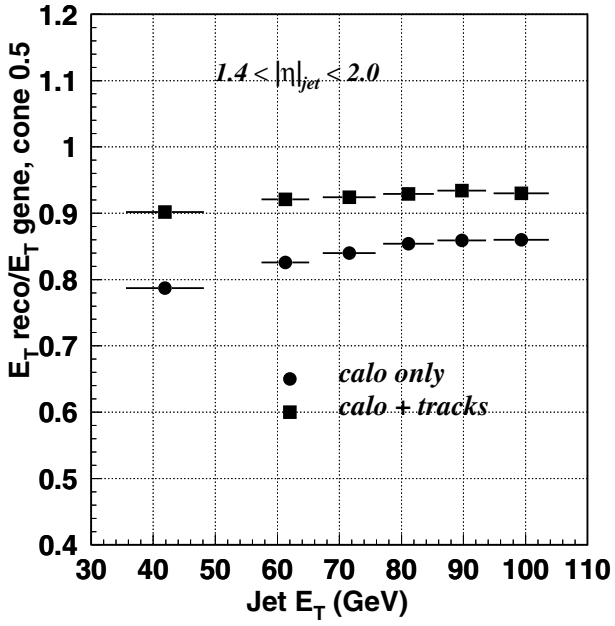

Fig. 15. Reconstructed jet transverse energy as a function of the generator jet transverse energy. The symbols are the same as in Fig. 14

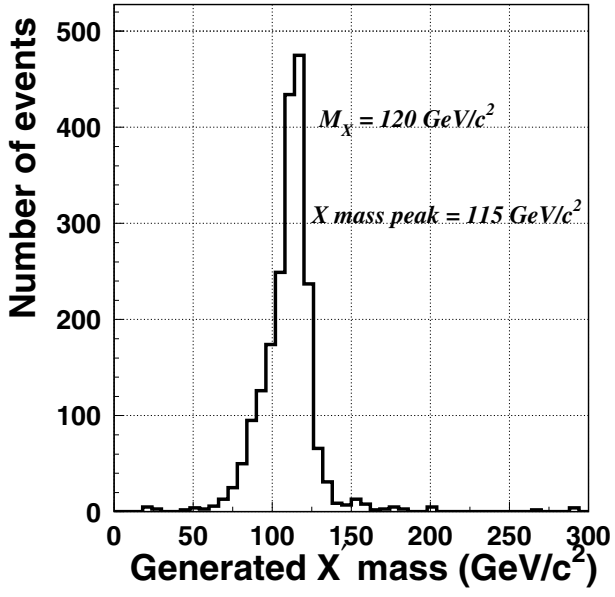

Fig. 16. Distribution of the X mass calculated with the two leading generator jets

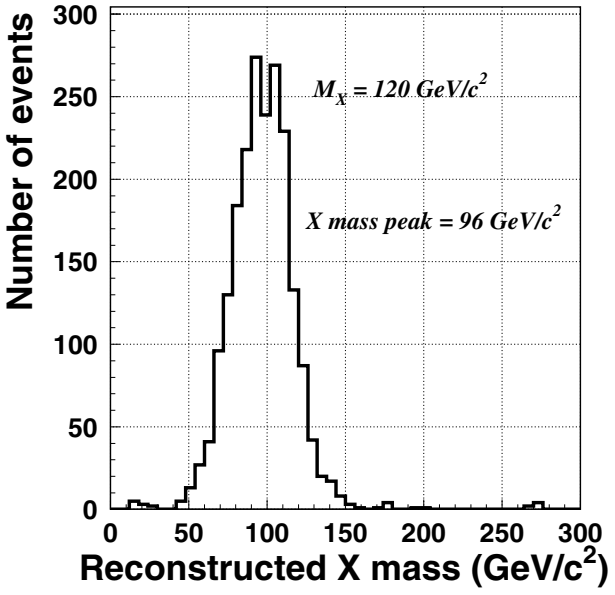

Fig. 17. Distribution of the reconstructed X mass determined with the two leading calorimeter jets

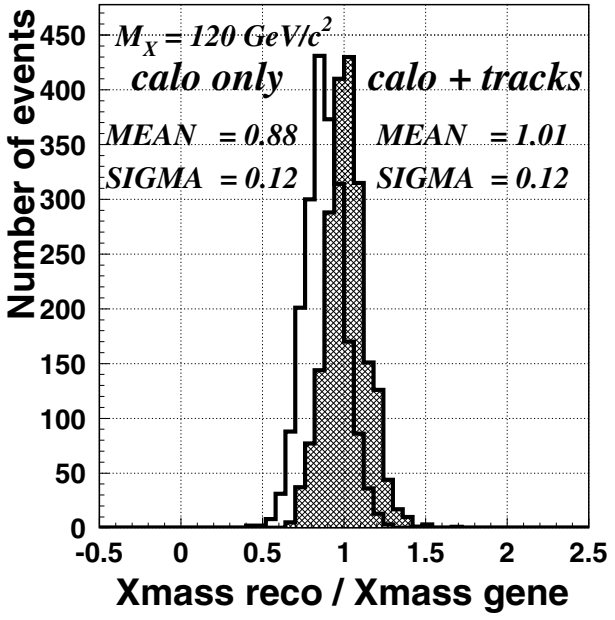

Fig. 18. Ratio of the reconstructed to the generated X mass with calorimeters only (empty histogram) and with calorimeter + tracks corrections (hatched histogram)

mate. Taking into account that pile-up events add on average ΔE $\approx$ 2.5 GeV [5] in a cone with $R = 0.5$ to the jet energy, the contribution of the pile-up energy to the mean reconstructed mass is estimated to be ≈ 5 GeV/c^2 ($< \mathrm{M_{pile-up}} > \approx \langle \mathrm{M} > +2\Delta\mathrm{E}$) assuming no correlations between the jet energies. After subtraction of the additional pile-up energy ($\approx$ 2.5 GeV) from the reconstructed jet energy, the ratio of the reconstructed to the generated masses is 0.84 and 0.97 before and after applying corrections, respectively.

3.2.4 Reconstruction of h(125 GeV) mass

One channel investigated at CMS is the gluon fusion into radion, $gg \to \phi \to hh \to \gamma\gamma b\bar{b}$, where one of the Higgs bosons decays into $b\bar{b}$. The mass of the latter can be determined from the corresponding reconstructed di-jet invariant mass. This channel was generated and digitized with low luminosity pile-up. The distribution of the di-jet mass reconstructed with the calorimeters only is shown in Fig. 19. Only jets with $|\eta| < 1.2$ and with good matching to the b quarks are considered. The mass of the Higgs

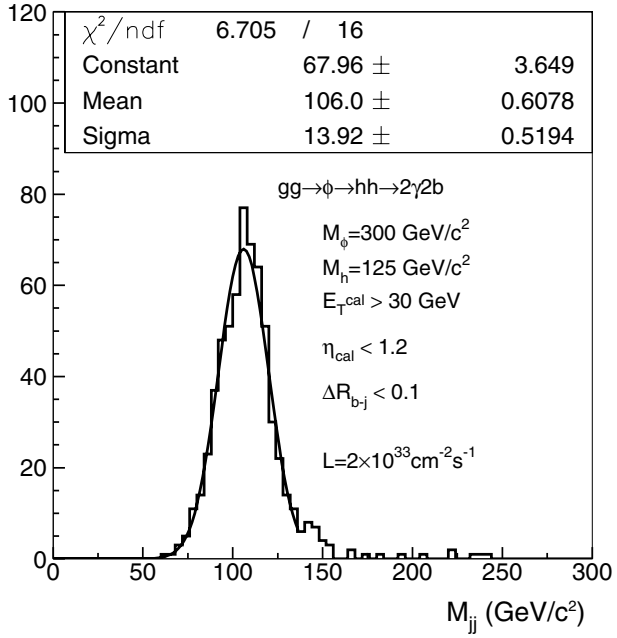

Fig. 19. Distribution of the Higgs boson mass determined from calorimeter jets in the hh $\rightarrow \gamma\gamma b\bar{b}$ channel

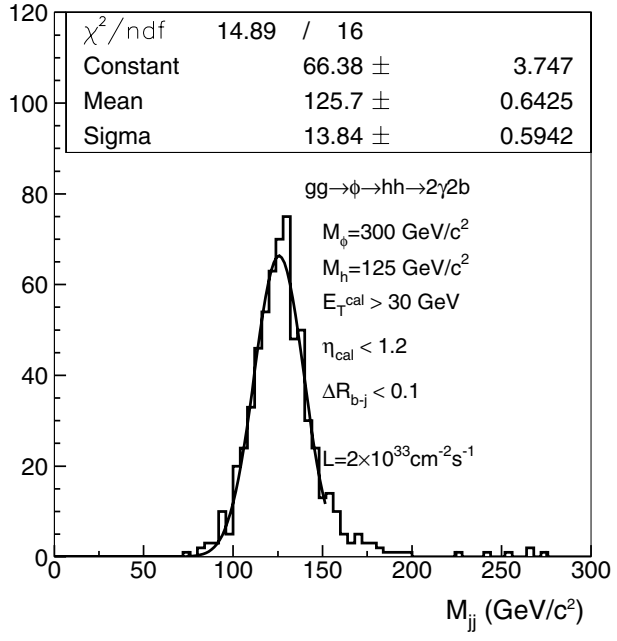

Fig. 20. Distribution of the Higgs mass determined from reconstructed jets using track corrections in the hh $\rightarrow \gamma\gamma b\bar{b}$ channel

boson is underestimated by about 20 GeV/c^2. The jet energy correction (Fig. 20) restores the mass scale and the resolution is improved from 13.2% to 11%.

4 Conclusion

Track information allows the jet energy resolution and linearity to be improved. For low energy jets (20 GeV), the resolution improves by a factor 1.7. For 100 GeV jets, the resolution improves by 15%. The non-linearity decreases by a factor two for low E_T jets and for high E_T jets (E_T >50 GeV), the ratio of $\langle \frac{E_T^{reco}}{E_T^{gene}} \rangle$ is 1.00 ± 0.04. This method has also been applied for reconstruction of the mass of di-jet systems (X $\rightarrow$ jj and h $\rightarrow$ bb). The correction almost completely restores the mass scale and the resolution is improved by 10%.

Acknowledgements. The authors wish to express their gratitude to S. Kunori and S. Eno for their interest and for fruitful discussions. They are also grateful to J. Rohlf and C. Tully for important comments and for helping with the text editing.

References

1. The LHC Study group. CERN/AC95-05-LHC
2. The Trigger and Data Aquisition Project, Vol. 2, Technical Design Report. CERN LHCC 2002-26, CMS TDR 6.2 (2002)
3. O. Kodolova, I. Vardanian, A. Oulianov, S. Kunori, CMS NOTE-2002/023 (2002)
4. D. Green, Energy Flow in CMS Calorimetry, Fermilab-FN-0709
5. A. Nikitenko, S. Kunori, R. Kinnunen, Missing transverse energy measurement with jet energy corrections. CMS NOTE 2001/040 (2001)
6. See for example ALEPH Coll, Nucl. Instrum. Methods A **360**, 481–506 (1995)
7. S. Lami, A. Bocci, S. Kuhlmann, G. Latino, FERMILAB-Conf-00/342-E CDF January 2001
8. M. Wing, Precise Mesurement of the Jet Energies with the ZEUS Detector. In: Proceedings of the IXth Int. Conf. on Calorimetry in Part. Phys., Annecy, Oct. 9–14 (2000)
9. D. Green et al., Energy Flow Objects and Usage of Tracks for Energy Measurement in CMS. CMS NOTE-2002/036 (2002)
10. CMS ECAL Technical Design Report, CERN/LHCC 97-33 (1997)
11. CMS HCAL Technical Design Report, CERN/LHCC 97-31 (1997)
12. CMS Technical Tracker Design Report, CERN/LHCC 98-6 (1998)
13. CMSIM user's Guide at www.http://cmsdoc.cern.ch/swsi.html
14. ORCA user's Guide at www.http://cmsdoc.cern.ch/swsi.html
15. V.V. Abramov et al., Studies of the response of the prototype CMS hadron calorimeter, including magnetic field effects, to pion, electron and muon beams. CMS NOTE 2000/003 (2000)
16. D. Green, Calibration of the CMS Calorimeter. Fermilab-FN-0704
17. C. Cucciarelli, M. Konecki, D. Kotlinski, T. Todorov, Track parameter evaluation and Primary Vertex Finding with pixel detector. CMS NOTE 2003/026
18. R. Wigmans, Nucl. Instrum. Methods A **265**, 273 (1988)
19. T. Sjostrand, Comput. Phys. Commun. **135**, 238 (2001)